Biotechnology and Bioengineering

WILEY

BIOTECHNOLOGY AND BIOENGINEERING

ARTICLE OPEN ACCESS

Establishment of a Single-Cell Minimal Medium: A Case Study for Microfluidic Cultivation of *Corynebacterium glutamicum*

Judith Wegmann[1] | Matthias Pesch[2] | Juliane Zwoch[3] | Andreas Schmid[3] | Dietrich Kohlheyer[2] | Alexander Grünberger[1]

[1]Institute of Process Engineering in Life Sciences, Karlsruhe Institute of Technology, Karlsruhe, Germany | [2]IBG-1: Institute of Bio- and Geosciences, Forschungszentrum Jülich GmbH, Jülich, Germany | [3]Department Solar Materials Biotechnology, Helmholtz Centre for Environmental Research (UFZ), Leipzig, Germany

Correspondence: Alexander Grünberger (alexander.gruenberger@kit.edu)

Received: 3 February 2026 | **Revised:** 27 March 2026 | **Accepted:** 30 March 2026

Funding: Deutsche Forschungsgemeinschaft, Grant/Award Number: 428038451

Keywords: Corynebacterium glutamicum | iron chelation | media establishment | microfluidics | minimal medium | single-cell cultivation | single-cell medium

ABSTRACT

Single-cell technologies are emerging as a complementary approach to conventional laboratory-scale cultivation setups. Particularly in microfluidic cultivation and screening, precisely controlled environmental conditions and defined minimal media become important for quantitative studies. Nevertheless, conventional bulk media optimized for other scales, are often employed despite differences in nutrient requirements across varying scales and cultivation modes. This study demonstrates the limitations of using bulk media for single-cell analysis of *Corynebacterium glutamicum* and highlights the need for revised minimal media for microfluidic cultivations under perfusion. The commonly used CGXII medium contains protocatechuic acid (PCA), which functions both as an iron chelator and a carbon source, thereby compromising its role as a minimal medium with one limiting substrate. We systematically evaluated alternative iron chelators to replace PCA using microfluidic single-cell cultivation. We show that not all chelators are applicable with *C. glutamicum* at the single-cell level and identify citrate as a suitable replacement that ensures iron availability without supporting growth in the absence of glucose. Based on these findings, we established a revised minimal medium, termed 'single-cell CGXII'. This medium was validated across different scales and enables robust, reproducible investigation of cellular physiology at single-cell resolution, improving accuracy and comparability in quantitative single-cell research.

1 | Introduction

Single-cell technologies have gained increasing attention in biotechnology and bioprocess development, particularly for screening, physiological characterization, and quantitative analysis of microbial systems (Anggraini et al. 2022; Deng et al. 2019). Within this field, microfluidic single-cell cultivation enables high-throughput studies with precise spatiotemporal control over the microenvironment of individual cells (Anggraini et al. 2022; Dusny and Grünberger 2020). In microfluidic systems under perfusion, cells are cultivated at extremely low biomass concentrations where secreted metabolites are continuously removed and cannot accumulate in the cultivation chamber, minimizing changes to both the local microenvironment and the surrounding medium (Grünberger et al. 2013; Song et al. 2024). A key advantage of microfluidics is

Judith Wegmann and Matthias Pesch contributed equally to this work.

thus the ability to quantify individual cellular responses to defined medium compositions across defined concentration ranges (Mustafi et al. 2012; Steinhoff et al. 2023; Täuber et al. 2022; Unthan et al. 2014). Under these conditions, buffering requirements, metabolite accumulation, and nutrient depletion differ fundamentally from batch or chemostat cultures (Täuber et al. 2021).

For quantitative single-cell experiments, defined cultivation media with clearly assigned functions of each component is essential. Minimal media are particularly suitable, as they support defined and controlled growth by fulfilling only the minimum nutrient demands. For the cultivation of *Corynebacterium glutamicum*, CGXII minimal medium is commonly used. *C. glutamicum* is a widely used organism with high relevance for biotechnological applications and an established model organism in systems biology (Becker and Wittmann 2020; Heider and Wendisch 2015; Wendisch 2020). CGXII contains protocatechuic acid (PCA), which was originally introduced as a chemically defined iron chelator to facilitate iron uptake by forming stable complexes with the metal (Keilhauer et al. 1993; Liebl et al. 1989). However, growth of *C. glutamicum* on PCA as sole carbon source as well as secondary substrate have been demonstrated beyond its role as chelator (Haußmann and Poetsch 2012; Lindemann et al. 2019; Merkens et al. 2005; Shen and Liu 2005; Unthan et al. 2014; Weiland et al. 2023). The co-metabolism of PCA next to glucose was demonstrated as biphasic growth in batch cultivations (Unthan et al. 2014), where a decline in the growth rate during the second phase of growth was attributed to the depletion of PCA, resulting in varying growth rates dependent on PCA availability as illustrated in Figure 1. While the co-metabolism of PCA is often negligible in conventional batch cultivations, its relevance increases under continuous perfusion conditions, where medium components cannot be depleted. Consequently, *C. glutamicum* maintains a steady growth rate within microfluidic cultivations under constant availability of PCA and glucose (Täuber et al. 2021; Unthan et al. 2014) (Figure 1). Under such conditions, the dual role of PCA as iron chelator and potential carbon source challenges the assumption of strictly defined single-carbon-source growth and complicates quantitative interpretation of growth and metabolic analyses.

Despite this, media formulations originally developed for bulk cultivation are widely used in microfluidic single-cell systems, often without critical reassessment of their suitability at very low cell numbers and under continuous perfusion. Thus, each medium component can be reconsidered with respect to its concentration, function, and necessity. Consequently, the increasing application of microbial single-cell analysis creates a

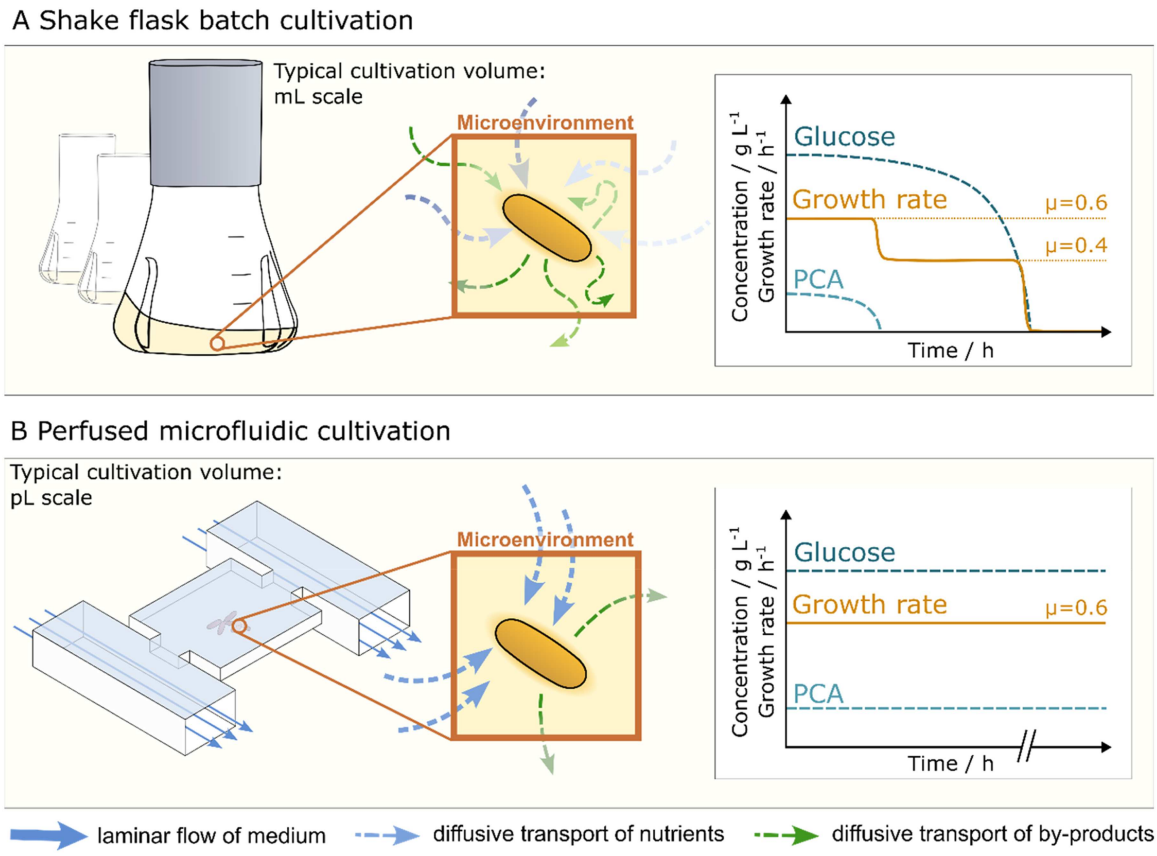

FIGURE 1 | Comparison of *C. glutamicum* growth in CGXII medium under batch and microfluidic cultivation conditions. (A) Batch cultures are characterized by transient conditions, including decreasing substrate concentrations and accumulation of secreted by-products with increasing biomass. Convective mixing and turbulent flow dominate mass transport while diffusion is only relevant in the immediate microenvironment of the cells. In CGXII medium, PCA is depleted within the first hours, resulting in a decrease in growth rate from $\mu = 0.6\,h^{-1}$ to $\mu = 0.4\,h^{-1}$ once glucose remains as the sole carbon source (see also (Unthan et al. 2014)). (B) Microfluidic single-cell cultivation provides constant microenvironments by continuous replenishment of nutrients and removal of by-products, resulting in stable growth rates at $\mu = 0.6\,h^{-1}$ throughout the cultivation duration. Nutrient supply and waste removal are governed by diffusion. Illustrations are not to scale.

demand for cultivation media that are specifically adapted to the nutritional and physiological requirements of individual cells. This enables a rational adjustment of media compositions when transferring cultivation strategies from bulk systems to microfluidic single-cell applications, ultimately improving physiological relevance and quantitative interpretability.

To address the limitations of PCA-supplemented CGXII medium, we systematically investigated alternative chemically defined iron chelators for *C. glutamicum* in single-cell experiments. Using microfluidic single-cell cultivation as the primary characterization platform complemented by batch cultivations, chelator compatibility and their impact on growth under defined carbon-source conditions were assessed. These analyses resulted in the establishment of a revised defined minimal medium that supports robust growth on glucose while employing an iron chelator that does not serve as an additional carbon source, thereby enabling controlled and quantitative single-cell studies.

2 | Material and Methods

2.1 | Bacterial Strain, Media Preparation and Preculture

All experiments were carried out with *C. glutamicum* wildtype ATCC 13032, cultivated in minimal CGXII medium based on (Keilhauer et al. 1993) with pH adjusted to 7. It consisted (per liter) of: 20 g $(NH_4)_2SO_4$, 5 g urea, 1 g K_2HPO_4, 1 g KH_2PO_4, 0.25 g $MgSO_4{\cdot}7H_2O$, 42 g 3-morpholinopropanesulfonic acid (MOPS), 13.2 mg $CaCl_2{\cdot}2H_2O$, 10 mg $FeSO_4{\cdot}7H_2O$, 10 mg $MnSO_4{\cdot}H_2O$, 1 mg $ZnSO_4{\cdot}7H_2O$, 0.31 mg $CuSO_4$, 0.02 mg $NiCl_2{\cdot}6H_2O$, 0.2 mg biotin, and 10 g glucose as carbon and energy source. For precultures in shaking flasks, 195 µM PCA was added as iron chelator. Dependent on the medium condition, the iron chelator was replaced by alternative iron chelators (ethylenediaminetetraacetic acid (EDTA), oxalate, malate, and citrate) in concentrations from 195 µM to 50 mM in microfluidic cultivations. Furthermore, the adapted medium with citrate as sole carbon source contained 5 mM $CaCl_2$ to increase citrate uptake. The medium components were prepared as separate stock solutions. The CGXII base, containing $(NH_4)_2SO_4$, urea, KH_2PO_4, K_2HPO_4, $MgSO_4{\cdot}7H_2O$, and MOPS, was adjusted to pH 7.0. $CaCl_2$ was added from a 13.2 g L^{-1} stock solution, biotin from a 0.2 g L^{-1} stock solution, and glucose from a 500 g L^{-1} stock solution. Trace elements were prepared as a 1000x stock solution adjusted to pH 1.0. Biotin and $CaCl_2$ were autoclaved, whereas all remaining stock solutions were sterile filtered before use. Iron chelators were generally added from 195 mM stock solutions. For 50 mM citrate conditions, however, citrate was added from a 650 mM stock solution. The final medium was prepared max. 24 h before use and was sterile filtered for microfluidic experiments to remove remaining particles. All chemicals were purchased from Carl Roth, Germany.

Shake flask cultivations were carried out in 100 mL baffled flasks with 10 mL working volume on a 120 rpm rotary shaker (25 mm diameter) at 30°C. For precultivation in shake flasks, cryo stocks were added to 37 g L^{-1} BHI (brain heart infusion, Becton Dickinson, USA) medium at pH 7.0 and transferred to CGXII medium with PCA after 8 h at an optical density (OD, at 600 nm) of 0.1. After approximately 15 h, the preculture was again transferred to freshly prepared CGXII medium as last preculture prior to chip cultivation and was inoculated with an OD of 0.2. The chip was inoculated with cells in the early exponential phase with an OD of approx. 0.5–1 to achieve fast and simple trapping of single cells.

2.2 | Microfluidic Cultivation

2.2.1 | *Chip Design*

The microfluidic chip consists of four separated similar systems, with eight channel arrays per system, and each array contains 40 growth chambers for microfluidic cultivation (Figure 2). The growth chambers are arranged in-between the media supply channels with a fluidic connection to both adjacent supply

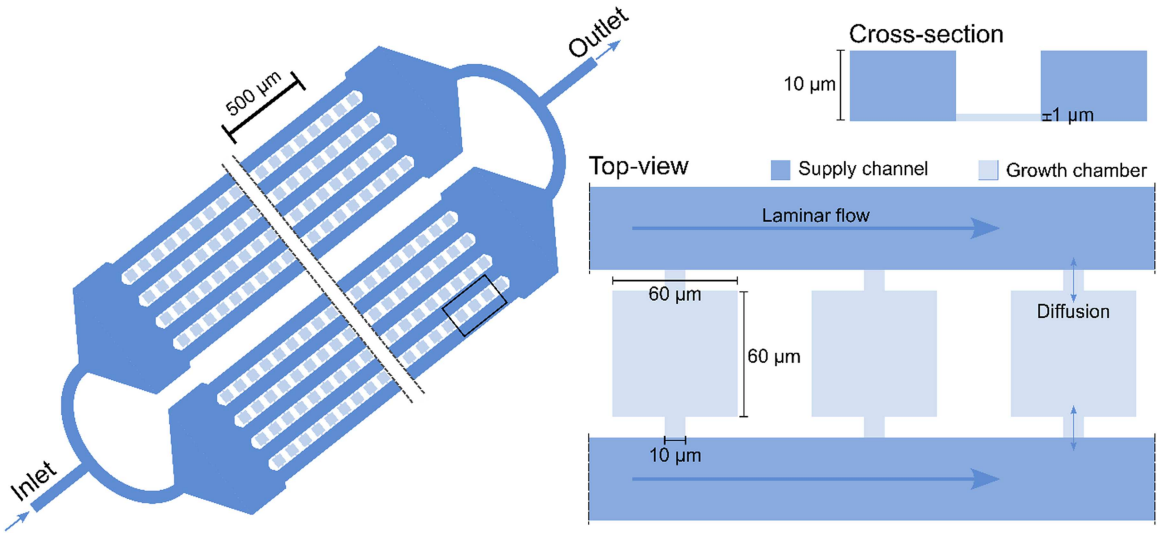

FIGURE 2 | Illustration of the chip design for microfluidic cultivation. Each microfluidic cultivation system consists of eight arrays which are arranged as pairs of four arrays. Medium is pumped via the inlet and is thereby transported through the supply channels to the growth chambers which are open on both sides to ensure sufficient nutrient supply via diffusion. Mass transport in the supply channels occurs via convective laminar flow, allowing for highly controlled conditions.

channels to ensure sufficient nutrient diffusion from the main supply channel with a height of 10 μm. Each monolayer chamber has dimensions of 60 × 60 × 1 μm (width × length × height). Supply channels are perfused with equal flow rates, resulting in solely diffusive mass transport inside the growth chambers.

2.2.2 | *Chip Fabrication*

The polydimethylsiloxane (PDMS) chips were replicated from a mold, which was fabricated in a two-layer photolithography process on a 4 inch silicon wafer (Gruenberger et al. 2013). The PDMS molding procedure according to (Blöbaum et al. 2023) is briefly described in the following section. PDMS was mixed in a 10:1 (w/w) ratio of base and linker (SYLGARD 184, DOW Europe GmbH, Germany) and poured on the master wafer. The PDMS coated wafer was degassed for 20 min under slight vacuum to remove air bubbles and baked for 2 h at 80°C. The inlets and outlets of the fabricated PDMS chips were punched with a 0.75 mm diameter biopsy puncher and cleaned with isopropanol before bonding. The PDMS chip and a glass substrate (0.175 mm thickness) were then oxygen plasma-treated to activate the surfaces of both objects (Diener electronic GmbH & Co. KG, Germany). Therefore, a vacuum was generated and oxygen was introduced until an oxygen atmosphere of 0.4 mbar was reached. The surfaces were then O_2 plasma treated for 36 s at 40% power supply. Subsequent bonding was strengthened by baking the bonded chip at 80°C for 2 min.

2.2.3 | *Microfluidic Cultivation*

For time-lapse imaging, the chip was mounted on an inverted microscope (Nikon Ti2 Eclipse, Japan) which was surrounded by an incubator (Cage incubator, OKO Touch, Okolab S.R.L., Italy) to ensure a constant temperature at 30°C. After inoculation and flushing, medium was pumped via Tygon tubing (Saint-Gobain ppl. Corp., Germany) with 300 nL min^{-1} (LA-120, Landgraf Laborsysteme HLL GmbH, Germany), ensuring continuous nutrient supply under perfusion mode. Single cells were analyzed in steady-state in perfusion mode as shown previously (Grünberger et al. 2012, 2013). Time-lapse images were taken every 10 to 15 min to monitor microbial growth and division behavior.

2.2.4 | *Time-Lapse Imaging and Data Analysis*

All microfluidic experiments were imaged by phase-contrast microscopy (Nikon DS-Qi2, Nikon, Netherlands) with a 100× oil immersion objective (CFI P-Apo DM Lambda, Nikon, Germany). Growth chambers used for time-lapse imaging were selected based on a low initial cell number and optimal centering of cells to facilitate image analysis. Colony growth was monitored for up to 24 h and analyzed using Omnipose-based segmentation with the bact_phase_omni model (Cutler et al. 2022; Seiffarth et al. 2024). Growth curves were fitted using linear regression in Python 3.12.8 using the linregress function implemented in the scipy. stats package. Growth rates were determined from the slope of the logarithmic cell count over time. To exclude non-exponentially growing colonies, a filtering criterion was applied which required a minimum duration of 5 h in the exponential phase with an $R^2 > 0.99$ for the linear fit. This was particularly important for conditions lacking glucose, where growth was often negligible. The area of single cells was calculated by the conversion factor of 0.07 μm px^{-1}. Data was analyzed and plotted using custom Python scripts (available at Supporting Information S14).

2.3 | Microtiter Plate Cultivation

Microtiter plate (MTP) cultivations were performed using the microbioreactor system BioLector XT (Beckman Coulter GmbH, USA). The online measurement of biomass, pH, and dissolved oxygen in a 48 well FlowerPlate (Beckman Coulter GmbH, USA) allows for parallel observation of multiple conditions in real-time. This setup enables high oxygen transfer rates and constant humidity.

The cells from the pre-culture were centrifuged and washed in CGXII medium without an iron chelator before inoculation to avoid the transfer of residual PCA. For each well, 1 mL cull suspension was inoculated with the desired dilution of the pre-culture and filled in the wells. Dilutions ranged from OD 1 to OD $1 \cdot 10^{-8}$ in steps of $1 \cdot 10^{-2}$, resulting in 5 dilution steps I-V. With the assumption that OD 1 corresponds to $1.31\text{-}2.60 \cdot 10^{8}$ cells mL^{-1} (Hartmann et al. 2021; Unthan et al. 2014), dilution V at OD $1 \cdot 10^{-8}$ should yield single-cell inocula with 1.31–2.60 cells mL^{-1}. The MTP was covered with a gas-permeable sealing foil (Beckman Coulter GmbH, USA) and cultivations were carried out in triplicates at 30°C and 1100 rpm with a shaking diameter of 3 mm. Biomass was measured as backscatter signal with gain 1. Growth data were blank-corrected, averaged over triplicates and analyzed by log-linear regression with a minimum of 20 data points and an $R^2 > 0.95$ to identify exponential growth phases using custom Python scripts (available at Supporting Information S14).

3 | Results and Discussion

3.1 | Evaluation of Alternative Iron Chelators Using PCA-Supplemented CGXII as Reference

To decouple iron availability from carbon metabolism under microfluidic perfusion conditions, PCA-supplemented CGXII was first evaluated as a reference and alternative iron chelators were systematically tested as potential substitutes. Iron chelation depends on specific functional groups, most commonly catechol-, hydroxamate-, or hydroxyl-containing compounds, which are characteristic features of siderophores and enable the formation of stable iron complexes (Johnstone and Nolan 2015; Köster 2001; Leventhal et al. 2019; Wilson et al. 2016; Winkelmann and Carrano 1997). PCA is classified as a hydroxybenzoic acid with a catechol moiety that efficiently scavenges ferric iron from the environment. However, PCA is also metabolized by *C. glutamicum* and contributes to cellular carbon metabolism as aromatic organic acids, including benzoic acids derivatives, are commonly degraded through the β-ketoadipate pathway (Chaudhry et al. 2007; Haußmann and Poetsch 2012; Kallscheuer et al. 2016; Shen and Liu 2005; Unthan et al. 2014). However, structural similarity and shared catabolic pathways do not necessarily translate into functional equivalence in iron acquisition. For instance, unsubstituted benzoic acid supports growth but lacks iron-reducing properties and does not function as an effective iron chelator (Haußmann et al. 2009; Müller et al. 2020), highlighting the need for careful selection of alternative chelators. Consequently, alternative iron

chelators must ensure sufficient cellular iron uptake without contributing to carbon metabolism under the applied cultivation conditions. Based on these structure-function considerations, different compounds with reported iron-binding properties were evaluated as potential replacements for PCA in microfluidic single-cell cultivation. Resulting growth rates obtained with PCA, EDTA, oxalate, malate, and citrate (each at 195 µM, equivalent to PCA concentration in standard CGXII) are summarized in Figure 3 (growth curves are provided in the Supporting Information Figure S2 to Figure S6).

As expected from previous studies, *C. glutamicum* was able to grow under microfluidic perfusion when PCA was added to the medium (Figure 3), confirming sufficient iron availability at the single-cell level. For parallel consumption of PCA and glucose, a mean growth rate of $\mu_{PCA} = 0.52 \pm 0.03\ h^{-1}$ was obtained, whereas growth on PCA as the sole carbon source yielded a lower mean growth rate of $\mu_{PCA\text{-}glc} = 0.29 \pm 0.06\ h^{-1}$. The reported growth rate of $\mu = 0.6\ h^{-1}$ for CGXII with glucose and PCA (Unthan et al. 2014) could not be reproduced, however growth on PCA as the sole carbon source exceeded previously reported values. These deviations are likely attributable to differences in pre-culture conditions as well as variations in data acquisition and growth quantification workflows (see Materials and Methods). In summary, cultivations with glucose as sole carbon source were not feasible, as iron supplementation relied on PCA, which was co-metabolized by *C. glutamicum*. While PCA reliably ensured iron uptake, its dual functionality compromised defined growth conditions with a single limiting carbon source under perfusion. This observation is consistent with secondary carbon source effects that are typically negligible in batch cultivations but become pronounced under continuous perfusion (Unthan et al. 2014). Consequently, an alternative iron chelator was required that separates iron chelation from carbon metabolism.

Several alternative iron chelators were subsequently evaluated under microfluidic single-cell perfusion to identify compounds fulfilling the defined requirements of iron availability without metabolic interference. Despite its widespread use as a chelating agent and ability to bind metal ions effectively (Eckert et al. 2022), EDTA failed to promote continuous growth in *C. glutamicum* in microfluidic single-cell cultivation, even in the presence of 10 g L^{-1} glucose. Although cells initiated growth within the growth chambers, none of the analyzed colonies fulfilled the predefined criteria (see Material and Methods, Supporting Information Figure S1), according to which a suitable iron chelator must support sustained and continuous exponential growth. This observation is consistent with the reported metal-sequestering and antimicrobial properties of EDTA (Paterson et al. 2023, 2025), which can impair essential metal homeostasis. Similarly, oxalate did not support continuous growth both in the presence and absence of glucose. Although oxalate can build stable iron complexes through its carboxylate group and has been associated with microbial iron transport (Dehner et al. 2010), these properties were insufficient to sustain

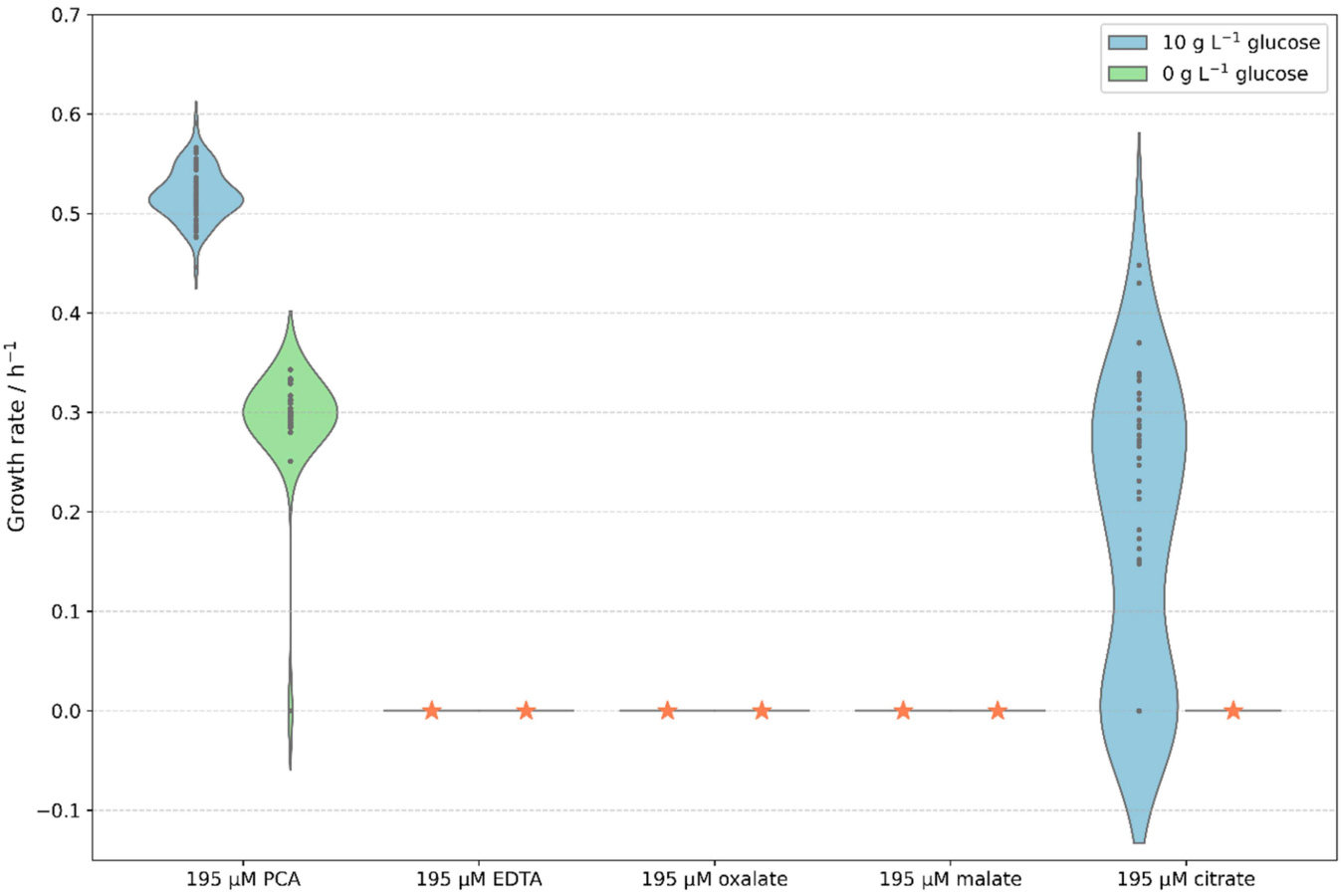

FIGURE 3 | Growth of *C. glutamicum* on 10 g L^{-1} glucose (blue) or in the absence of glucose (green) with 195 µM iron chelator for different potential iron chelators in microfluidic single-cell cultivations. Continuous growth was defined as exponential growth maintained for a minimum duration of 5 h with a linear fit of $R^2 > 0.99$. Stars indicate conditions in which none of the colonies fulfilled the criteria for continuous growth ($\mu = 0$).

growth under continuous perfusion. Subsequently, malate was assessed as a potential replacement for PCA but also failed to support growth irrespective of glucose availability. While growth on malate was observed in batch cultivations, previous studies have shown that malate can inhibit glucose utilization through down-regulation of central glucose consumption pathways (Vasco-Cárdenas et al. 2013), which likely contributes to its incompatibility under the applied conditions. Finally, citrate was tested as iron-complexing compound. While unable to serve as a sole carbon source at these concentrations, citrate supported growth when combined with glucose. Despite a pronounced heterogeneity across colonies in the growth chambers (as indicated from violin plot distribution), a mean growth rate of $\mu_{195\ \mu M\ cit} = 0.18 \pm 0.14\ h^{-1}$ was obtained in microfluidic cultivations. Continuous growth, according to the applied growth criteria (see Material & Methods), was observed in 66% of analyzed colonies ($\mu_{195\ \mu M\ cit,\ growing} = 0.27 \pm 0.08\ h^{-1}$ for growing colonies), whereas growth in the remaining growth chambers was insufficient or discontinuous ($\mu = 0$). This heterogeneous cellular response indicates that citrate-mediated iron supply is functional but not uniformly effective at this concentration. The ability of citrate to form stable metal complexes and its role as an iron carrier have been previously documented in other organisms such as *Aspergillus niger* under iron-limited conditions (Odoni et al. 2017). Moreover, citrate-based siderophores have been shown to play a significant role in microbial iron acquisition (Johnstone and Nolan 2015; Winkelmann and Carrano 1997).

These results indicate that iron-chelating compounds are not universally compatible with *C. glutamicum* and cannot substitute for PCA under the conditions applied for microfluidic single-cell analysis. Among the tested compounds, citrate was the only chelator that supported growth in the presence of glucose without being exclusively consumed. Consequently, citrate demonstrated the greatest potential and was selected as the most suitable candidate for further investigations.

3.2 | Citrate as Non-Metabolized Iron Chelator

In the next step, PCA was replaced by citrate as iron chelator in microfluidic single-cell cultivations. Cellular growth was analyzed for increasing citrate concentrations from 975 µM to 11.12 mM in the presence and absence of 10 g L^{-1} glucose to systematically evaluate its influence on growth (Figure 4, growth curves in the Supporting Information Figure S7 to Figure S10).

Citrate supplementation resulted in a concentration-dependent increase in growth rate in the presence of glucose, with maximal growth observed at intermediate concentrations (Figure 4). A fivefold increase from 195 µM to 975 µM citrate led to a 189% increase in mean growth rates ($\mu_{975\ \mu M\ cit} = 0.34 \pm 0.03\ h^{-1}$ compared to $\mu_{195\ \mu M\ cit} = 0.18 \pm 0.14\ h^{-1}$, Figure 3) and a more homogenous growth response across all growth chambers, as indicated by the violin plot distribution. The highest mean

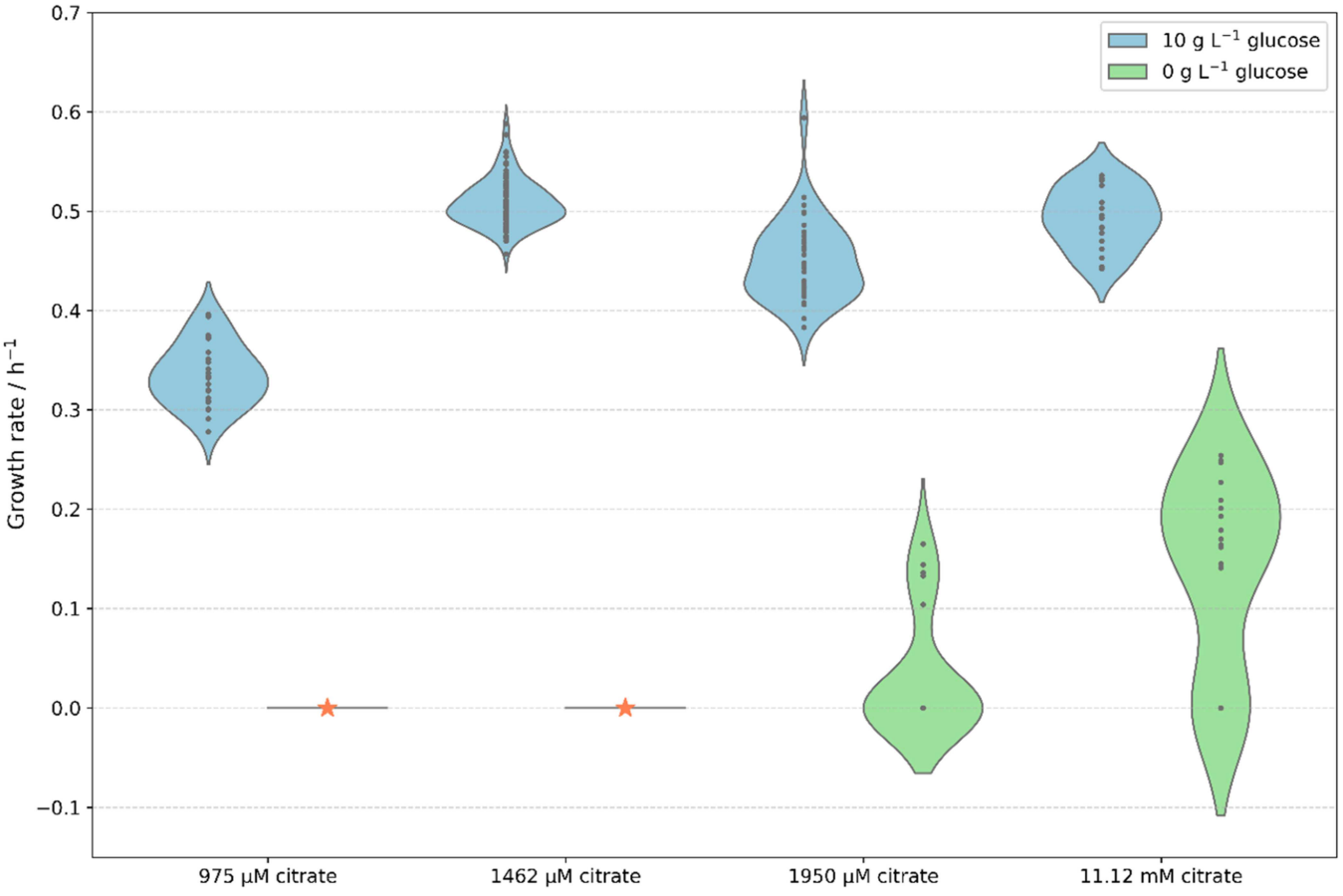

FIGURE 4 | Growth of *C. glutamicum* on both 10 g L^{-1} (blue) and 0 g L^{-1} (green) glucose with different citrate concentrations ranging from 975 µM to 11.12 mM citrate in microfluidic single-cell cultivations. Continuous growth was defined as exponential growth maintained for a minimum duration of 5 h with a linear fit of $R^2 > 0.99$. Stars indicate conditions in which none of the colonies fulfilled the criteria for continuous growth ($\mu = 0$).

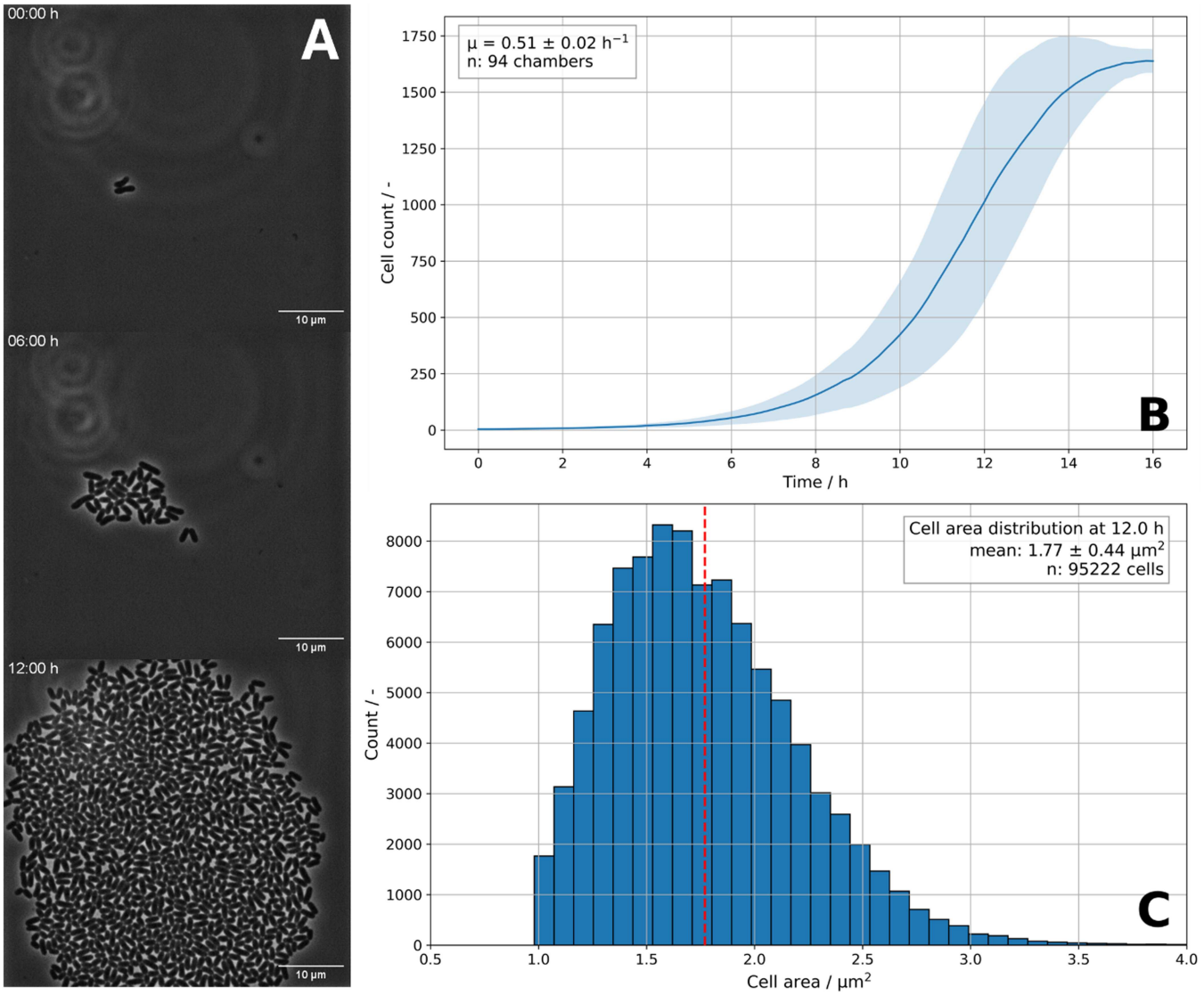

FIGURE 5 | Growth of *C. glutamicum* on 10 g L^{-1} glucose supplemented with 1462 µM citrate. (A) Growth of cells in an exemplary microfluidic growth chamber for three different timepoints at 0, 6 and 12 h. (B) The cell count over time with exponentially growing cells averaged for all 94 analyzed growth chambers. A decrease of the cell count after approx. 15 h corresponds to the maximal number of cells that fit in a growth chamber. (C) Distribution of the single-cell area at 12 h displayed in a histogram. The red line represents the overall mean.

growth rate ($\mu_{1462\ \mu M\ cit} = 0.51 \pm 0.02\ h^{-1}$) was observed at 1462 µM citrate (7.5-fold increase) under glucose-containing conditions. A further increase by 10-fold to 1950 µM did not further enhance growth ($\mu_{1950\ \mu M\ cit} = 0.45 \pm 0.04\ h^{-1}$), indicating saturation of citrate-mediated iron acquisition.

In the absence of glucose, growth remained negligible at citrate concentrations below 1950 µM (Figure 4), suggesting that citrate primarily functioned as an iron chelator under these conditions. However, heterogeneous colony growth behavior emerged at 1950 µM citrate and revealed two distinct growth patterns. While the majority did not show any signs of exponential growth under glucose-free conditions, the violin plot distribution indicates that a fraction of cells (upper distribution of data points in the violin plot, 24% of tracked colonies with $\mu_{1950\ \mu M\ cit,\ growing} = 0.14 \pm 0.02\ h^{-1}$) was still able to initiate exponential growth despite the absence of the main carbon source. At higher citrate concentrations of 11.12 mM (57-fold increase), growth rates of $\mu_{11.12\ mM\ cit} = 0.49 \pm 0.03\ h^{-1}$ were observed in the presence of glucose. Under glucose-free conditions, exponential growth occurred in 72% of growth chambers ($\mu_{11.12\ mM\ cit\text{-}glc,\ growing} = 0.20 \pm 0.04\ h^{-1}$) with a mean growth rate of $\mu_{11.12\ mM\ cit\text{-}glc} = 0.14 \pm 0.10\ h^{-1}$, suggesting measurable metabolic contribution of citrate at elevated concentrations. These results align with previous reports of minor growth at high citrate concentrations (Liebl et al. 1989).

Based on these results, 1462 µM citrate was identified as the optimal concentration for a revised 'single-cell CGXII' medium, supporting high growth under glucose-containing conditions while minimizing metabolic interference in the absence of glucose. Representative growth characteristics from microfluidic cultivations are shown in Figure 5, demonstrating consistent rod-shaped morphology, uniform growth behaviour across all analyzed colonies and narrow cell size distributions (mean cell area of $1.77 \pm 0.44\ \mu m^2$). Variations in the cell area result from small cells

after division and elongated apically growing cells just before division (Messelink et al. 2021; Nieto et al. 2023). The observed cell size distribution aligns with previously reported characteristics of *C. glutamicum*, indicating that the citrate-based medium maintains normal cell morphology (Messelink et al. 2021; Neumeyer et al. 2013; Nieto et al. 2023).

The 'single-cell CGXII' with 1462 μM citrate was successfully applied in microfluidic cultivations, yielding growth and morphological characteristics comparable to those obtained with the conventional CGXII composition. Furthermore, the results show that the carbon source and iron chelator can be identical, since both PCA (Figure 3) and highly concentrated citrate (Figure 4) enabled growth without glucose addition. This shows that *C. glutamicum* can also utilize citrate simultaneously as a carbon source and chelator. Consequently, either compound can also serve as the sole growth-supporting substrate when defined single-substrate growth is desired. This allows precise analysis of carbon source-specific growth and facilitates strictly controlled single-substrate experiments in the microfluidic cultivation system.

3.3 | Growth on Citrate as Sole Carbon Source

Building on the observation that citrate can support growth in the absence of glucose, we next systematically investigated its capacity to sustain continuous growth as the sole carbon source in microfluidic perfusion conditions. Previous studies reported growth rates comparable to PCA-supplemented media when citrate is supplied at high concentrations and suggested enhanced citrate consumption as a carbon source (Liebl et al. 1989; Von Der Osten et al. 1989). This effect appears particularly pronounced when citrate is supplied as sodium citrate, where high ion availability enhances citrate uptake through synergistic uptake mechanisms (Brocker et al. 2009).

These observations align with the known regulatory and transport characteristics of citrate metabolism in *C. glutamicum*. Unlike other bacteria, *C. glutamicum* shows no catabolite repression when glucose and citrate are present, allowing simultaneous consumption of both substrates (Brocker et al. 2009; Polen et al. 2007). Two primary citrate uptake systems have been identified (Polen et al. 2007), both belonging to the transporter families that mediate symport of citrate with divalent cations such as Mg^{2+}, Ca^{2+} or Sr^{2+} (Bott and Brocker 2012; Brocker et al. 2009; Frunzke and Bott 2008). Expression of these transport systems is strongly induced during growth on citrate with notably higher mRNA levels for iron-siderophore transport systems compared to PCA-supplemented conditions (Polen et al. 2007). Enhanced citrate uptake has therefore been associated with increased formation of metal-citrate complexes and elevated divalent ion availability (Brocker et al. 2009; Polen et al. 2007), with maximal growth previously observed by supplementing 5 mM of $CaCl_2$ (Bott and Brocker 2012). In contrast to these earlier observations, our results indicate that standard CGXII ion concentrations (0.09 mM $CaCl_2$) combined with elevated citrate levels are already sufficient for citrate utilization in most of the growth chambers analyzed. Growth rates up to $\mu_{11.12\ mM\ cit\text{-}glc,\ growing} = 0.20\ h^{-1}$ were observed at 11.12 mM citrate in the absence of glucose (Figure 4), suggesting the presence of additional uptake mechanisms. Enhanced uptake may result from steep concentration gradients across the cellular membrane with facilitated diffusive transport (Koster 2005) or from continuous replenishment of divalent ions during perfusion.

To directly distinguish citrate concentration-dependent effects from ion-mediated uptake, citrate-supported growth was subsequently analyzed under conditions of elevated ion availability to strongly induce the described transporter systems for citrate uptake and utilization. Based on previous reports, experiments were first conducted at 50 mM citrate in the presence of 5 mM $CaCl_2$, followed by a reduction of the citrate concentration to 1462 μM while maintaining identical ion conditions. Growth was analyzed both in the presence and absence of glucose (Figure 6). All growth curves are depicted in the Supporting Information (Figure S11 and Figure S12).

Under elevated ion availability, comparable growth was observed for both citrate concentrations. At 1462 μM citrate with 5 mM $CaCl_2$, cells exhibited high and continuous growth rates of $\mu_{1462\ \mu M\ cit+CaCl2+glc} = 0.56 \pm 0.04\ h^{-1}$ in the presence and $\mu_{1462\ \mu M\ cit+CaCl2-glc} = 0.47 \pm 0.04\ h^{-1}$ in the absence of glucose. These results demonstrate that even low citrate concentrations support growth when Ca^{2+} levels are sufficient to promote citrate uptake and utilization. Similarly, growth on 50 mM citrate as the sole carbon source yielded a mean growth rate of $\mu_{50mM\ cit+Cacl2-glc} = 0.42 \pm 0.04\ h^{-1}$ and confirmed earlier observations (Polen et al. 2007). The addition of glucose further increased growth to $\mu_{50mM\ cit+CaCl2+glc} = 0.54 \pm 0.02\ h^{-1}$, again indicating combined carbon source utilization and supporting previous findings of enhanced growth on citrate-glucose mixtures (Polen et al. 2007).

By omitting glucose, citrate serves simultaneously as the sole carbon source for biomass formation and as an iron chelator. Nevertheless, growth rates remained slightly reduced compared to conditions combining citrate and elevated ion availability with glucose, under which the highest growth rates of this study were achieved ($\mu \approx 0.55\ h^{-1}$). This difference indicates that although citrate alone is sufficient to sustain continuous exponential growth, the simultaneous availability of glucose provides an additional metabolic advantage. Importantly, increasing the citrate concentration did not result in an increase in growth rates in continuous cultivations. Within the tested conditions, these observations indicate that ion availability rather than citrate concentration was the primary factor enabling efficient citrate uptake and utilization, highlighting the need to carefully consider ion composition when designing defined cultivation media.

The glucose-free citrate medium, however, provides a markedly more defined cultivation environment as citrate functions as the sole carbon source. A key constraint of this minimal formulation is its dependence on citrate as the only carbon source, which inherently restricts carbon-source flexibility and therefore limits its use in studies that require alternative substrates. Moreover, retransfer of this medium to batch cultivations may pose challenges for pH control, as extensive uptake of citric acid can substantially affect medium acidity.

3.4 | Application of 'Single-Cell CGXII' for Different Inoculum Densities

Given these limitations, subsequent experiments were conducted using the glucose-based 'single-cell CGXII', which supports growth exclusively on glucose. To evaluate the applicability of the newly developed medium not only in microfluidic cultivation, but also with standard microwell-based

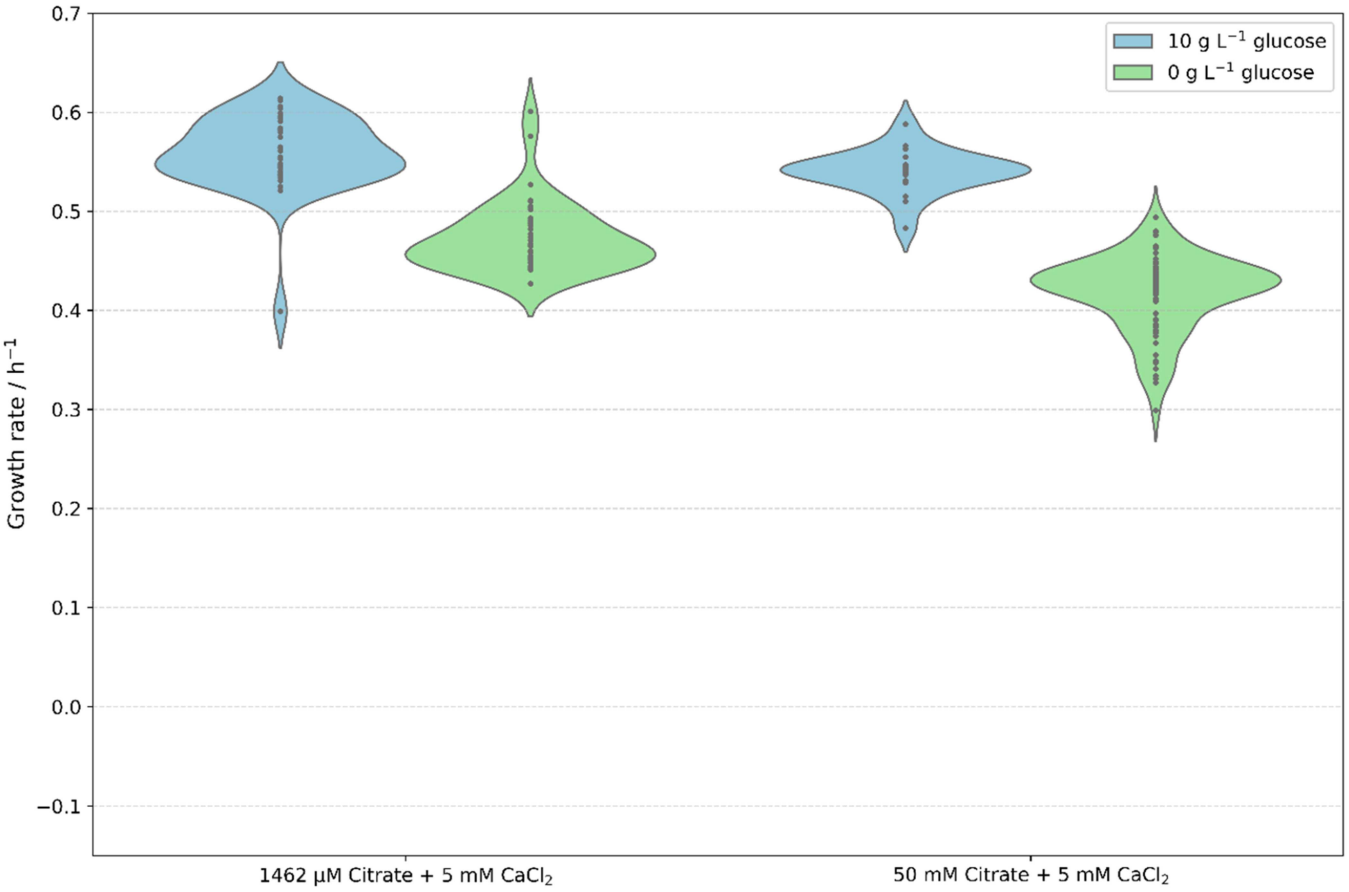

FIGURE 6 | Growth of *C. glutamicum* on 50 mM citrate together with 10 g L^{-1} glucose (blue) or as sole carbon source and 0 g L^{-1} glucose (green). The ion concentration was further increased to 5 mM $CaCl_2$ for all conditions. Criteria for continuous growth were set to exponential growth for a minimum duration of 5 h with an $R^2 > 0.99$ for the linear fit.

screening formats, it was transferred to a MTP cultivation. Such transferability is particularly critical for workflows that combine fluorescence-activated cell sorting-based isolation of single cells with subsequent regrowth in microwells (Binder et al. 2012; Riba et al. 2016), where reliable outgrowth from extremely low inocula is essential to maintain screening fidelity and minimize false-negative recovery events.

Therefore, serial dilution experiments down to inocula containing only a few viable *C. glutamicum* cells per well were performed to assess growth in CGXII medium supplemented with either 195 µM PCA, 1462 µM citrate, or no iron chelator. Initial cell densities were stepwise reduced from OD 1 ($\approx 1.31–2.60 \cdot 10^8$ cells mL^{-1}) down to OD $1 \cdot 10^{-8}$ ($\approx 1.31–2.60$ cells mL^{-1}) (Hartmann et al. 2021; Unthan et al. 2014) to assess the influence of nutrient availability per cell. Growth behavior and fitted growth curves are shown in Figure 7 and highlight the differences between the tested iron chelators and the necessity of iron complexation for *C. glutamicum* growth.

Cultures supplemented with PCA exhibited the highest specific growth rates (Figure 7A), consistent with previous literature (Thoma et al. 2023). The mean specific growth rate in the exponential phase ($\mu_{PCA,\ MTP} = 0.41\ h^{-1}$) was independent of the initial cell density, highlighting that no medium limitations influenced microbial growth. A similar effect can be identified for the supplementation of citrate which resulted in slightly lower mean growth rates of ($\mu_{cit,\ MTP} = 0.33\ h^{-1}$) and a delayed onset of exponential growth compared to PCA. This temporal delay may be attributed to PCA's assumed role as growth initiator (Liebl et al. 1989; Müller et al. 2020; Thoma et al. 2023; Unthan et al. 2014). Compared to microfluidic cultivation (Figure 3 and Figure 4), growth rates in the MTP were consistently lower and decreased from 0.52 to 0.41 h^{-1} for PCA (−21%) and from 0.51 to 0.33 h^{-1} for citrate (−35%). This likely reflects fundamental differences in the cultivation mode (Grünberger et al. 2013). In the microfluidic system, continuous medium perfusion ensures constant nutrient supply and simultaneous removal of metabolic by-products, thereby maintaining stable extracellular microenvironments for each cell. In contrast, MTP cultivations are batch-based and therefore subject to temporal changes in nutrient availability, oxygen availability and metabolite accumulation. Additionally, decreasing inoculum size in the MTP cultivations led to extended lag phases and delayed detection of backscatter signals for both chelators, resulting in time-shifted but parallel plots. Even at extreme dilutions ($\approx 1.31–2.60$ cells mL^{-1}), cultures managed to initiate exponential growth after approximately 30 h, demonstrating that population growth can be initiated from (very few) single viable cells. Increased variability between replicates at these dilutions likely reflects differences in initial cell number and cell-cycle states.

In contrast, cultures without iron chelator supplementation showed strongly impaired growth (Figure 7B). Only cultures

Dilution	I	II	III	IV	V
Estimated Cells mL^{-1}	1.31-2.60·10^{8}	1.31-2.60·10^{6}	1.31-2.60·10^{4}	131-260	1.31.-2.60

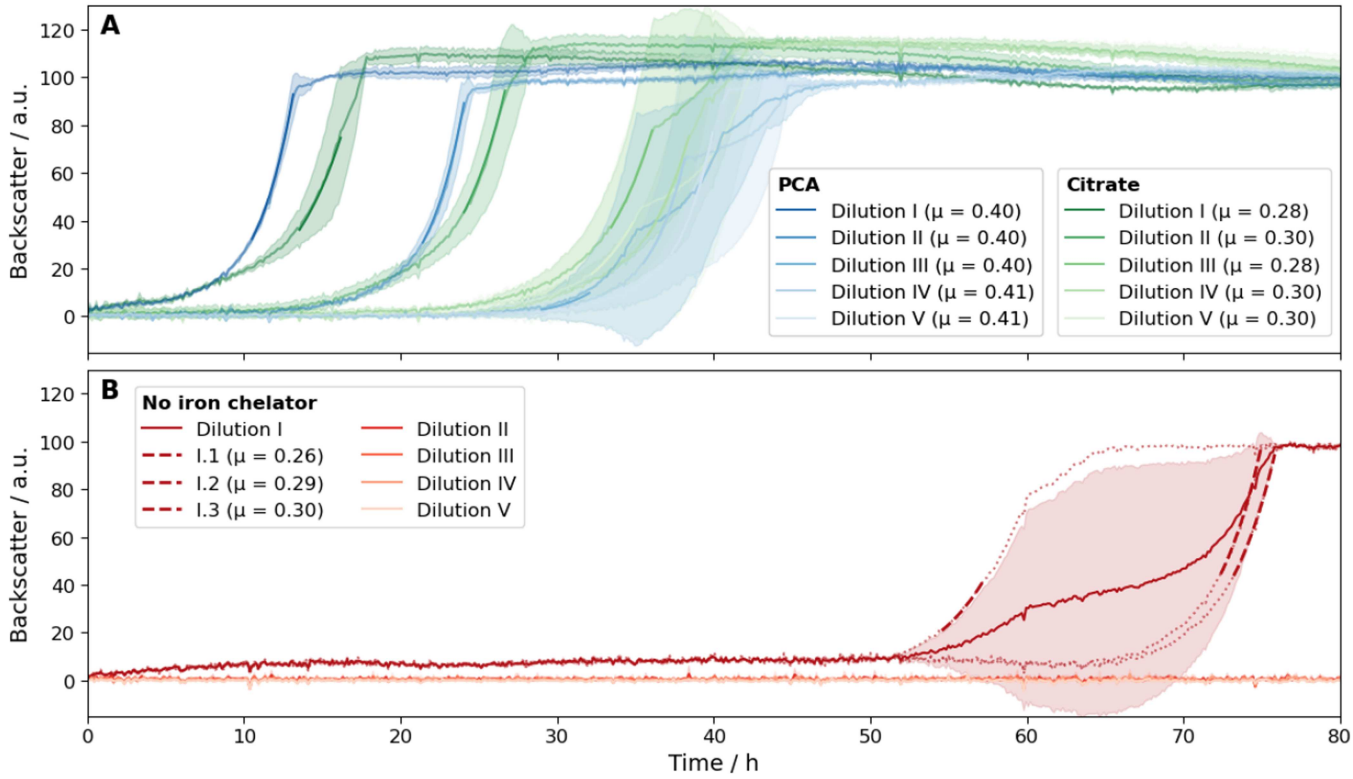

FIGURE 7 | Microtiter plate cultivations with varying supplementation of the iron chelator and increasing dilution of the inoculum from OD 1 at dilution I to OD $1 \cdot 10^{-8}$ at dilution V, shown as averaged triplicates with corresponding standard deviation. Each curve was fitted with the criteria of minimum 20 data points and $R^2 > 0.95$ to obtain specific growth rates with the fit range depicted by the solid line. (A) Supplementation of CGXII medium with 195 μM PCA (blue tones) or 1462 μM citrate (green tones). (B) Cultivations without the addition of an iron chelator for the different inoculum levels. Only cultures with a starting OD of 1 (dilution I) could initiate growth and meet the fitting requirements. Due to the different timepoints of exponential growth, each of the triplicates (dotted lines) is additionally displayed with a single fit.

inoculated at OD 1 were able to overcome the lag phase and started exponential growth after approximately 50 h of cultivation. The pronounced variability between replicates indicates severe physiological stress, likely reflecting time-consuming cellular adaptation to overcome the present iron limitation. Interestingly, cultures with an initial OD of 1 showed a slight but consistent increase in backscatter in the first hours of cultivation, followed by a prolonged plateau for over 50 h before growth resumed. This observation suggests transient buffering of iron demand until synthesis or alternative uptake systems are upregulated, potentially through intracellular or surface-bound iron reserves (Kawashima et al. 2023; Küberl et al. 2020; Wennerhold and Bott 2006). *C. glutamicum* might also release chelating metabolites to reduce iron, accumulating enough to collectively solubilize iron at high cell densities. The late initiation of growth could be further attributed to iron (chelator) scavenging from lysed cells at higher inoculum densities, providing a transient nutrient pulse ('necromass') (Jin 2023).

Lower dilutions (dilution II-V) failed to show any significant increase in backscatter even after 160 h of cultivation (see Supporting Information Figure S13) despite high nutrient availability per cell. These findings indicate persistent iron limitation, either due to insufficient iron uptake or because produced chelator concentrations remained too low and too diluted to meet the iron demand of small populations. Together, these observations support the idea that a critical biomass density is required to alleviate iron limitation above a certain threshold to overcome iron scarcity in CGXII medium without chelator supplementation.

Overall, these results underscore the essential role of iron chelators for robust growth initiation at low cell densities. The successful transfer of the glucose-based 'single-cell CGXII' medium to an MTP-based cultivation format demonstrates its reliable applicability across different cultivation scales and experimental workflows. This revised medium therefore establishes a robust foundation for investigating and screening individual cells under defined minimal conditions. Moreover, the development strategy presented here may serve as a blueprint for generating additional single-cell-compatible minimal media tailored to other microbial systems.

4 | Conclusion

Standard CGXII medium for *C. glutamicum* contains PCA to accelerate iron uptake from the environment. While originally introduced solely as an iron chelator, the role of PCA has extended beyond its primary function and also acts as a metabolizable carbon source. This dual functionality is largely masked in batch cultivations but becomes critical under continuous perfusion, where both primary and secondary carbon sources are continuously available. Therefore, defined single-carbon-source conditions are compromised, complicating quantitative studies of metabolism, cellular regulation and carbon source utilization in microfluidic single-cell cultivations.

To address this limitation, alternative iron chelators were systematically evaluated. Among the tested organic acids, citrate emerged as the most suitable replacement, as it supported glucose-based growth without serving as a carbon source under standard cultivation conditions. While concentrations equivalent to PCA were insufficient to promote growth, intermediate concentrations below 1950 μM citrate enabled high growth rates without evidence of metabolic contribution. At higher concentrations, saturation effects and indications of citrate utilization were observed. A citrate concentration of 1462 μM citrate was identified as optimal: It yields high growth rates ($\mu \approx 0.5\ h^{-1}$ with glucose) while showing no experimental evidence of acting as a carbon source on its own. The observed influence of divalent ion availability further highlights the role of ion-dependent transport processes in citrate uptake and utilization. These findings demonstrate that ion availability rather than citrate concentration significantly influences its functionality in cultivations with *C. glutamicum*, likely via ion symporter-mediated transport. Replacing glucose may however not be feasible in most applications due to its established role as efficient and economical carbon source with well-characterized metabolic pathways. Validation of the revised 'single-cell CGXII' in MTP batch cultivations demonstrated robust and reproducible growth across cultivation scales and modes, even at very low cell densities.

By eliminating the secondary carbon source, the revised 'single-cell CGXII' medium enables quantitative growth and metabolic studies with improved data interpretability and accurate mass balancing. Beyond its practical applicability, these findings provide valuable insights into citrate transport and utilization in *C. glutamicum* under continuous cultivation and highlight the complexity of nutrient uptake mechanisms across cultivation modes. Overall, this comprehensive evaluation emphasizes the importance of critically reassessing medium composition when transferring cultivation strategies from bulk to microfluidic single-cell systems. Medium components and their concentration must be carefully reconsidered and adapted to the specific nutrient demands of single cells. These principles are not limited to the present system but are broadly applicable to the design of defined media for other organisms and cultivation platforms.

Author Contributions

Judith Wegmann: Conceptualization, investigation, methodology, formal analysis, visualization, writing – original draft, writing – review and editing. **Matthias Pesch:** Conceptualization, investigation, methodology, formal analysis, writing – review and editing. **Juliane Zwoch:** Conceptualization, writing – review and editing. **Andreas Schmid:** Supervision, funding acquisition, writing – review and editing. **Dietrich Kohlheyer:** Supervision, funding acquisition, writing – review and editing. **Alexander Grünberger:** Conceptualization, supervision, funding acquisition, writing – review and editing.

Acknowledgments

Judith Wegmann, Alexander Grünberger, Matthias Pesch, Dietrich Kohlheyer, Juliane Zwoch and Andreas Schmid gratefully acknowledge the German Research Foundation (Deutsche Forschungsgemeinschaft (DFG)) for providing funding for priority program SPP 2170 'Interzell' (project no. 428038451). Open Access funding enabled and organized by Projekt DEAL.

Conflicts of Interest

The authors declare no conflicts of interest.

Data Availability Statement

Preprocessed data obtained from image analysis (see Material and Methods), analysis workflow and visualization of results are accessible in the Supporting Information S14.

References

Anggraini, D., N. Ota, Y. Shen, et al. 2022. "Recent Advances in Microfluidic Devices for Single-Cell Cultivation: Methods and Applications." *Lab on a Chip* 22, no. 8: 1438–1468. https://doi.org/10.1039/D1LC01030A.

Becker, J., and C. Wittmann. 2020. "Pathways at Work: Metabolic Flux Analysis of the Industrial Cell Factory Corynebacterium glutamicum." In *Corynebacterium glutamicum*, edited by In. M. Inui and K. Toyoda, 23, 227–265. Springer International Publishing. https://doi.org/10.1007/978-3-030-39267-3_8.

Binder, S., G. Schendzielorz, N. Stäbler, et al. 2012. "A High-Throughput Approach to Identify Genomic Variants of Bacterial Metabolite Producers at the Single-Cell Level." *Genome Biology* 13, no. 5: R40. https://doi.org/10.1186/gb-2012-13-5-r40.

Blöbaum, L., S. Täuber, and A. Grünberger. 2023. "Protocol to Perform Dynamic Microfluidic Single-Cell Cultivation of C. glutamicum." *STAR Protocols* 4, no. 3: 102436. https://doi.org/10.1016/j.xpro.2023.102436.

Bott, M., and M. Brocker. 2012. "Two-Component Signal Transduction in Corynebacterium glutamicum and Other Corynebacteria: On the Way Towards Stimuli and Targets." *Applied Microbiology and Biotechnology* 94, no. 5: 1131–1150. https://doi.org/10.1007/s00253-012-4060-x.

Brocker, M., S. Schaffer, C. Mack, and M. Bott. 2009. "Citrate Utilization by *Corynebacterium glutamicum* Is Controlled by the CitAB Two-Component System Through Positive Regulation of the Citrate Transport Genes *citH* and *tctCBA*." *Journal of Bacteriology* 191, no. 12: 3869–3880. https://doi.org/10.1128/JB.00113-09.

Chaudhry, M. T., Y. Huang, X.-H. Shen, A. Poetsch, C.-Y. Jiang, and S.-J. Liu. 2007. "Genome-Wide Investigation of Aromatic Acid Transporters in Corynebacterium glutamicum." *Microbiology* 153, no. 3: 857–865. https://doi.org/10.1099/mic.0.2006/002501-0.

Cutler, K. J., C. Stringer, T. W. Lo, et al. 2022. "Omnipose: A High-Precision Morphology-Independent Solution for Bacterial Cell Segmentation." *Nature Methods* 19, no. 11: 1438–1448. https://doi.org/10.1038/s41592-022-01639-4.

Dehner, C. A., J. D. Awaya, P. A. Maurice, and J. L. DuBois. 2010. "Roles of Siderophores, Oxalate, and Ascorbate in Mobilization of Iron From Hematite by the Aerobic Bacterium *Pseudomonas mendocina*." *Applied and Environmental Microbiology* 76, no. 7: 2041–2048. https://doi.org/10.1128/AEM.02349-09.

Deng, Y., A. Finck, and R. Fan. 2019. "Single-Cell Omics Analyses Enabled by Microchip Technologies." *Annual Review of Biomedical Engineering* 21, no. 1: 365–393. https://doi.org/10.1146/annurev-bioeng-060418-052538.

Dusny, C., and A. Grünberger. 2020. "Microfluidic Single-Cell Analysis in Biotechnology: From Monitoring Towards Understanding." *Current Opinion in Biotechnology* 63: 26–33. https://doi.org/10.1016/j.copbio.2019.11.001.

Eckert, S., E. J. Mascarenhas, R. Mitzner, et al. 2022. "From the Free Ligand to the Transition Metal Complex: FeEDTA– Formation Seen at Ligand K-Edges." *Inorganic Chemistry* 61, no. 27: 10321–10328. https://doi.org/10.1021/acs.inorgchem.2c00789.

Frunzke, J., and M. Bott. 2008. "Regulation of iron homeostasis in Corynebacterium glutamicum." In *Corynebacteria: Genomics and molecular biology*, edited by In. A. Burkovski, 241–266. Caister Academic Press. https://www.caister.com/cory.

Gruenberger, A., C. Probst, A. Heyer, W. Wiechert, J. Frunzke, and D. Kohlheyer. 2013. "Microfluidic Picoliter Bioreactor for Microbial Single-Cell Analysis: Fabrication, System Setup, and Operation." *Journal of Visualized Experiments: JoVE* 6, no. 82: 50560. https://doi.org/10.3791/50560.

Grünberger, A., J. Van Ooyen, N. Paczia, et al. 2013. "Beyond Growth Rate 0.6: *Corynebacterium glutamicum* Cultivated in Highly Diluted Environments." *Biotechnology and Bioengineering* 110, no. 1: 220–228. https://doi.org/10.1002/bit.24616.

Grünberger, A., N. Paczia, and C. Probst, et al. 2012. "A Disposable Picolitre Bioreactor for Cultivation and Investigation of Industrially Relevant Bacteria on the Single Cell Level." *Lab on a Chip* 12, no. 11: 2060. https://doi.org/10.1039/c2lc40156h.

Hartmann, F. S. F., I. Anastasiou, T. Weiß, J. Shen, and G. M. Seibold. 2021. "Impedance Flow Cytometry for Viability Analysis of Corynebacterium glutamicum." *Journal of Microbiological Methods* 191: 106347. https://doi.org/10.1016/j.mimet.2021.106347.

Haußmann, U., and A. Poetsch. 2012. "Global Proteome Survey of Protocatechuate- and Glucose-Grown Corynebacterium glutamicum Reveals Multiple Physiological Differences." *Journal of Proteomics* 75, no. 9: 2649–2659. https://doi.org/10.1016/j.jprot.2012.03.005.

Haußmann, U., S. W. Qi, D. Wolters, M. Rögner, S. J. Liu, and A. Poetsch. 2009. "Physiological Adaptation of *Corynebacterium glutamicum* to Benzoate as Alternative Carbon Source—A Membrane Proteome-Centric View." *Proteomics* 9, no. 14: 3635–3651. https://doi.org/10.1002/pmic.200900025.

Heider, S. A. E., and V. F. Wendisch. 2015. "Engineering Microbial Cell Factories: Metabolic Engineering of *Corynebacterium glutamicum* With a Focus on Non-Natural Products." *Biotechnology Journal* 10, no. 8: 1170–1184. https://doi.org/10.1002/biot.201400590.

Jin, Q. 2023. "Building Microbial Kinetic Models for Environmental Application: A Theoretical Perspective." *Applied Geochemistry* 158: 105782. https://doi.org/10.1016/j.apgeochem.2023.105782.

Johnstone, T. C., and E. M. Nolan. 2015. "Beyond Iron: Non-Classical Biological Functions of Bacterial Siderophores." *Dalton Transactions* 44, no. 14: 6320–6339. https://doi.org/10.1039/C4DT03559C.

Kallscheuer, N., M. Vogt, J. Kappelmann, et al. 2016. "Identification of the phd Gene Cluster Responsible for Phenylpropanoid Utilization in Corynebacterium glutamicum." *Applied Microbiology and Biotechnology* 100, no. 4: 1871–1881. https://doi.org/10.1007/s00253-015-7165-1.

Kawashima, K., T. Nagakubo, N. Nomura, and M. Toyofuku. 2023. "Iron Delivery Through Membrane Vesicles in Corynebacterium glutamicum." *Microbiology Spectrum* 11, no. 3: e01222-23. https://doi.org/10.1128/spectrum.01222-23.

Keilhauer, C., L. Eggeling, and H. Sahm. 1993. "Isoleucine Synthesis in Corynebacterium glutamicum: Molecular Analysis of the ilvB-ilvN-ilvC Operon." *Journal of Bacteriology* 175, no. 17: 5595–5603. https://doi.org/10.1128/jb.175.17.5595-5603.1993.

Köster, W. 2001. "ABC Transporter-Mediated Uptake of Iron, Siderophores, Heme and Vitamin B12." *Research in Microbiology* 152, no. 3–4: 291–301. https://doi.org/10.1016/S0923-2508(01)01200-1.

Koster, W. 2005. "Cytoplasmic Membrane Iron Permease Systems in the Bacterial Cell Envelope." *Frontiers in Bioscience* 10, no. 1–3: 462. https://doi.org/10.2741/1542.

Küberl, A., A. Mengus-Kaya, T. Polen, and M. Bott. 2020. "The Iron Deficiency Response of Corynebacterium glutamicum and a Link to Thiamine Biosynthesis." *Applied and Environmental Microbiology* 86, no. 10: e00065-20. https://doi.org/10.1128/AEM.00065-20.

Leventhal, G. E., M. Ackermann, and K. T. Schiessl. 2019. "Why Microbes Secrete Molecules to Modify Their Environment: The Case of Iron-Chelating Siderophores." *Journal of the Royal Society Interface* 16, no. 150: 20180674. https://doi.org/10.1098/rsif.2018.0674.

Liebl, W., R. Klamer, and K.-H. Schleifer. 1989. "Requirement of Chelating Compounds for the Growth of Corynebacterium glutamicum in Synthetic Media." *Applied Microbiology and Biotechnology* 32, no. 2: 205–210. https://doi.org/10.1007/BF00165889.

Lindemann, D., C. Westerwalbesloh, D. Kohlheyer, A. Grünberger, and E. von Lieres. 2019. "Microbial Single-Cell Growth Response at Defined Carbon Limiting Conditions." *RSC Advances* 9, no. 25: 14040–14050. https://doi.org/10.1039/c9ra02454a.

Merkens, H., G. Beckers, A. Wirtz, and A. Burkovski. 2005. "Vanillate Metabolism in Corynebacterium glutamicum." *Current Microbiology* 51, no. 1: 59–65. https://doi.org/10.1007/s00284-005-4531-8.

Messelink, J. J., F. Meyer, M. Bramkamp, and C. P. Broedersz. 2021. "Single-Cell Growth Inference of Corynebacterium glutamicum Reveals Asymptotically Linear Growth." *eLife* 10: e70106. https://doi.org/10.7554/eLife.70106.

Müller, F., J. Rapp, A.-L. Hacker, A. Feith, R. Takors, and B. Blombach. 2020. "CO_2/HCO_3^- Accelerates Iron Reduction Through Phenolic Compounds." *mBio* 11, no. 2: e00085-20. https://doi.org/10.1128/mBio.00085-20.

Mustafi, N., A. Grünberger, D. Kohlheyer, M. Bott, and J. Frunzke. 2012. "The Development and Application of a Single-Cell Biosensor for the Detection of l-Methionine and Branched-Chain Amino Acids." *Metabolic Engineering* 14, no. 4: 449–457. https://doi.org/10.1016/j.ymben.2012.02.002.

Neumeyer, A., T. Hübschmann, S. Müller, and J. Frunzke. 2013. "Monitoring of Population Dynamics of *Corynebacterium glutamicum* by Multiparameter Flow Cytometry." *Microbial Biotechnology* 6, no. 2: 157–167. https://doi.org/10.1111/1751-7915.12018.

Nieto, C., S. Täuber, L. Blöbaum, Z. Vahdat, A. Grünberger, and A. Singh. 2025. "Coupling Bacterial Cell Size Regulation With Clonal Proliferation Dynamics Reveals Cell Division Based on Surface Area." *bioRxiv* 1: 573217. https://doi.org/10.1101/2023.12.26.573217.

Odoni, D. I., M. P. Van Gaal, T. Schonewille, et al. 2017. "Aspergillus niger Secretes Citrate to Increase Iron Bioavailability." *Frontiers in Microbiology* 8: 1424. https://doi.org/10.3389/fmicb.2017.01424.

Von Der Osten, C. H., C. Gioannetti, and A. J. Sinskey. 1989. "Design of a Defined Medium for Growth of Corynebacterium glutamicum in Which Citrate Facilitates Iron Uptake." *Biotechnology Letters* 11, no. 1: 11–16. https://doi.org/10.1007/BF01026778.

Paterson, J. R., J. M. Wadsworth, P. Hu, and G. J. Sharples. 2023. "A Critical Role for Iron and Zinc Homeostatic Systems in the Evolutionary Adaptation of Escherichia coli to Metal Restriction." *Microbial Genomics* 9, no. 12: 001153. https://doi.org/10.1099/mgen.0.001153.

Paterson, J. R., J. M. Wadsworth, and R. J. Lee, et al. 2025. "Enhanced Resistance of Metal Sequestering Agents by Reconfiguration of the Staphylococcus aureus Cell Wall." *Npj Antimicrobials and Resistance* 3, no. 1: 61. https://doi.org/10.1038/s44259-025-00131-1.

Polen, T., D. Schluesener, A. Poetsch, M. Bott, and V. F. Wendisch. 2007. "Characterization of Citrate Utilization in *Corynebacterium glutamicum* by Transcriptome and Proteome Analysis." *FEMS Microbiology Letters* 273, no. 1: 109–119. https://doi.org/10.1111/j.1574-6968.2007.00793.x.

Riba, J., T. Gleichmann, S. Zimmermann, R. Zengerle, and P. Koltay. 2016. "Label-Free Isolation and Deposition of Single Bacterial Cells From Heterogeneous Samples for Clonal Culturing." *Scientific Reports* 6, no. 1: 32837. https://doi.org/10.1038/srep32837.

Seiffarth, J., T. Scherr, B. Wollenhaupt, et al. 2024. "ObiWan-Microbi: OMERO-Based Integrated Workflow for Annotating Microbes in the Cloud." *SoftwareX* 26: 101638. https://doi.org/10.1016/j.softx.2024.101638.

Shen, X., and S. Liu. 2005. "Key Enzymes of the Protocatechuate Branch of the Beta-Ketoadipate Pathway for Aromatic Degradation in Corynebacterium glutamicum." *Science in China. Series C, Life Sciences* 48, no. 3: 241–249. https://doi.org/10.1007/BF03183617.

Song, Y., J. Yin, W. E. Huang, B. Li, and H. Yin. 2024. "Emerging Single-Cell Microfluidic Technology for Microbiology." *TrAC, Trends in Analytical Chemistry* 170: 117444. https://doi.org/10.1016/j.trac.2023.117444.

Steinhoff, H., M. Finger, M. Osthege, et al. 2023. "Experimental kS Estimation: A Comparison of Methods for Corynebacterium glutamicum From Lab to Microfluidic Scale." *Biotechnology and Bioengineering* 120, no. 5: 1288–1302. https://doi.org/10.1002/bit.28345.

Täuber, S., L. Blöbaum, V. Steier, M. Oldiges, and A. Grünberger. 2022. "Microfluidic Single-Cell Scale-Down Bioreactors: A Proof-of-Concept for the Growth of Corynebacterium glutamicum at Oscillating pH Values." *Biotechnology and Bioengineering* 119, no. 11: 3194–3209. https://doi.org/10.1002/bit.28208.

Täuber, S., J. Schmitz, L. Blöbaum, N. Fante, H. Steinhoff, and A. Grünberger. 2021. "How to Perform a Microfluidic Cultivation Experiment—A Guideline to Success." *Biosensors* 11, no. 12: 485. https://doi.org/10.3390/bios11120485.

Thoma, F., C. Appel, D. Russ, J. Huber, F. Werner, and B. Blombach. 2023. "Improving Growth Properties of Corynebacterium glutamicum by Implementing an Iron-Responsive Protocatechuate Biosynthesis." *Microbial Biotechnology* 16, no. 5: 1041–1053. https://doi.org/10.1111/1751-7915.14244.

Unthan, S., A. Grünberger, J. van Ooyen, et al. 2014. "Beyond Growth Rate 0.6: What Drives Corynebacterium glutamicum to Higher Growth Rates in Defined Medium." *Biotechnology and Bioengineering* 111, no. 2: 359–371. https://doi.org/10.1002/bit.25103.

Vasco-Cárdenas, M. F., S. Baños, A. Ramos, J. F. Martín, and C. Barreiro. 2013. "Proteome Response of Corynebacterium glutamicum to High Concentration of Industrially Relevant C4 and C5 Dicarboxylic Acids." *Journal of Proteomics* 85: 65–88. https://doi.org/10.1016/j.jprot.2013.04.019.

Weiland, F., N. Barton, M. Kohlstedt, J. Becker, and C. Wittmann. 2023. "Systems Metabolic Engineering Upgrades Corynebacterium glutamicum to High-Efficiency cis, cis-Muconic Acid Production From Lignin-Based Aromatics." *Metabolic Engineering* 75: 153–169. https://doi.org/10.1016/j.ymben.2022.12.005.

Wendisch, V. F. 2020. "Metabolic Engineering Advances and Prospects for Amino Acid Production." *Metabolic Engineering* 58: 17–34. https://doi.org/10.1016/j.ymben.2019.03.008.

Wennerhold, J., and M. Bott. 2006. "The DtxR Regulon of *Corynebacterium glutamicum*." *Journal of Bacteriology* 188, no. 8: 2907–2918. https://doi.org/10.1128/JB.188.8.2907-2918.2006.

Wilson, B. R., A. R. Bogdan, M. Miyazawa, K. Hashimoto, and Y. Tsuji. 2016. "Siderophores in Iron Metabolism: From Mechanism to Therapy Potential." *Trends in Molecular Medicine* 22, no. 12: 1077–1090. https://doi.org/10.1016/j.molmed.2016.10.005.

Winkelmann, G. and Carrano, C. J., ed. 1997. *Transition Metals in Microbial Metabolism*, 1st ed.). Harwood Academic Publishers.

Supporting Information

Additional supporting information can be found online in the Supporting Information section.
Supporting File 1: bit70203-sup-0001-Supporting_FIGURES1_to_S13.
Supporting File 2: bit70203-sup-0002-SupMat.